Journal of The Electrochemical Society, **148** (3) C197-C202 (2001)
0013-4651/2001/148(3)/C197/6/$7.00 © The Electrochemical Society, Inc.

Electron-Beam Induced Nanomasking for Metal Electrodeposition on Semiconductor Surfaces

T. Djenizian,* L. Santinacci,*,[a] and P. Schmuki**

Department of Materials Science, LKO, University of Erlangen-Nuremberg, D-91058 Erlangen, Germany

The present work investigates the masking effect of carbon contamination patterns deposited by the electron-beam (E-beam) of a scanning electron microscope (SEM) for metal electrodeposition reactions. Carbon contamination lines were written at different electron doses on n-type Si(100) surfaces. Subsequently Au was electrochemically deposited from a 1 M KCN + 0.01 M $KAu(CN)_2$ solution on the E-beam treated surface sites. The carbon masks as well as the Au deposits were characterized by SEM, atomic force microscopy, and scanning Auger electron spectroscopy. We demonstrate that carbon deposits in the order of 1 nm thickness can be sufficient to achieve a negative resist effect, *i.e.*, can block the electrodeposition of Au completely selectively. The lateral resolution of the process is in the sub-100 nm range. The nucleation and growth of Au deposits and their morphology as well as the selectivity and resolution of the process depend on several factors such as the electron dose during masking, and the applied potential and polarization time during Au deposition. The process opens new perspectives for selective electrodeposition, *i.e.*, for high definition patterning of surfaces with a wide range of materials.
 [DOI: 10.1149/1.1348258]

Manuscript submitted March 14, 2000; revised manuscript received December 5, 2000.

During past decades, there has been a great deal of interest in micro- and nanometer scale pattern generation on semiconductors. The field is particularly driven by semiconductor technology and its continuous demand for shrinking dimensions in the development of established devices [such as metal oxide semiconductor field effect transistors (MOSFETs[1])] as well as for the creation of novel devices (such as quantum effect devices[2]). Therefore, a range of techniques bearing the potential to achieve submicrometer resolution have been studied and established. Except for UV lithography, electron beam (E-beam) lithography is currently one of the most employed approaches to achieve high resolution patterning of conventional poly(methyl methacrylate) (PMMA) photoresists, on one hand to fabricate photolithographic masks[3] and on the other hand to create ultrasmall linewidths on both Si and SiO_2.[4-8] Other lithographic techniques are based on the exposure of photoresists to X-rays,[3] focused ion beams,[3,9] or employ scanning probe methods.[10] Direct writing approaches using electron or ion beams are much less reported. A number of studies deal with E-beam or ion beam induced deposition reactions. The principle is that precursor vapor species (*e.g.*, metallorganic compounds) are introduced into the vacuum chamber of the instrument where, under the direct ion- or electron bombardment, the precursor molecules decompose and form a deposit on the substrate surface. Such E-beam and ion-beam induced deposition has been used to create 3-D nanostructures[11-13] in the 1-100 nm range or to directly generate different single electron transistors or superconducting quantum interference devices (SQUIDs).[14]

A specific and well known case of E-beam induced patterning is the formation of carbon rich contamination layers in scanning electron microscopes (SEMs). The E-beam activates reactions of the residual hydrocarbons (molecules from the pump oil) in diffusion pumped systems to create a highly cross-linked hydrocarbon deposit. It has been reported that such deposits can successfully be applied as a mask for subsequent ion milling leading to ultrasmall structures.[15] Characterization work on carbonaceous deposits in SEM chambers showed that hydrocarbons adsorbed on a substrate surface are decomposed by the E-beam and form diamond-like carbon (DLC) an amorphous structure of carbon having mechanical and electrical properties close to diamond[16,17]

The present work explores possibilities to use C-masks produced by contamination writing in a SEM to suppress selectively metal electrodeposition at treated surface locations and thus to provide the basis for a novel patterning method in the submicrometer range.

From a technological point of view, metal/semiconductor junctions are essential for microelectronic devices. Hence, over the past 20 years, metal deposition on semiconductor surfaces by sputter deposition or evaporation techniques have been widely studied. Electrochemical deposition of metals on semiconductors has recently found renewed interest.[18-24] Due to its advantages and performance, electrodeposition has been adopted by the semiconductor industry, *e.g.*, to deposit copper for on-chip interconnections leading to a decreasing resistance and reducing process complexity.[25-27] In order to achieve selective electrodeposition, masking approaches based on conventional lithography or new developments such as the LIGA technique have been applied. Apart from approaches based on masking, electrochemical reactions can become localized if local differences in the substrate reactivity exist. For example, it has been shown that porous silicon growth can electrochemically be initiated preferentially at surface defects created in an n-type substrate by Si^{2+} focused ion beam bombardment[28] or that metal deposition can be achieved selectively at native defects of a single crystalline substrate surface such as single atomic steps.[29,30]

Within the present work, Au deposition on a contamination patterned Si(100) surface is studied in order to achieve insights in the feasibility and limits of the negative patterning potentials of such C-masks.

Experimental

Experiments were carried out on n-type silicon (100) wafers with a resistivity of 1 to 10 Ω cm. Prior to experiments, a layer of 1 μm thermal SiO_2 was grown on the wafers. Into this SiO_2 layer, arrays of square openings of 400 × 400 μm were etched by classical photolithography. (This prepatterning was carried out to facilitate locating the nanostructures subsequently deposited into the openings.) The patterned wafers were cleaved to samples of 2 × 2 cm, each one carrying five square openings. The samples were then degreased by sonicating in acetone, isopropanol, and methanol, rinsed with deionized water and dried in an argon stream. To hydrogen passivate the surface within the square openings, the samples were immersed into 1% HF for 1 min. To achieve E-beam induced deposition of C-line patterns, the samples were treated within the open squares with the ''horizontal'' single line mode in a Philips XL-30 FEG SEM. During the deposition the pressure of the chamber was $3 \cdot 10^{-6}$ mbar, the voltage was set to 20 kV and the E-beam current was 40 pA. All lines were written using the manufacturers aperture number 4. Different electron dose exposures were achieved by varying the exposure time under a constant electron current.

* Electrochemical Society Student Member.
** Electrochemical Society Active Member.
[a] On leave from: EPFL Lausanne, Department of Materials Science, LTP, Switzerland.

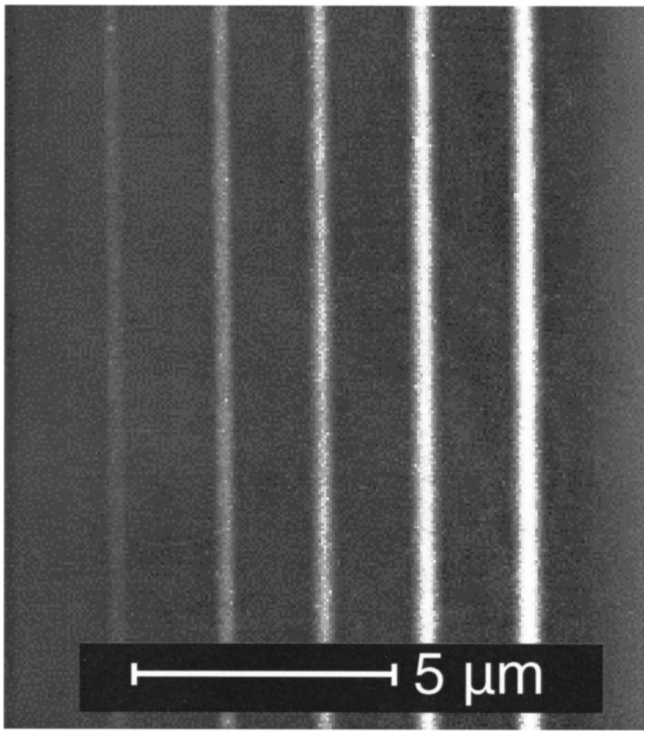

Figure 1. AFM top view of an array of five contamination lines E-beam deposited on silicon with 10, 30, 60, 120, and 180 s exposure time (the exposure time increases from the left to the right).

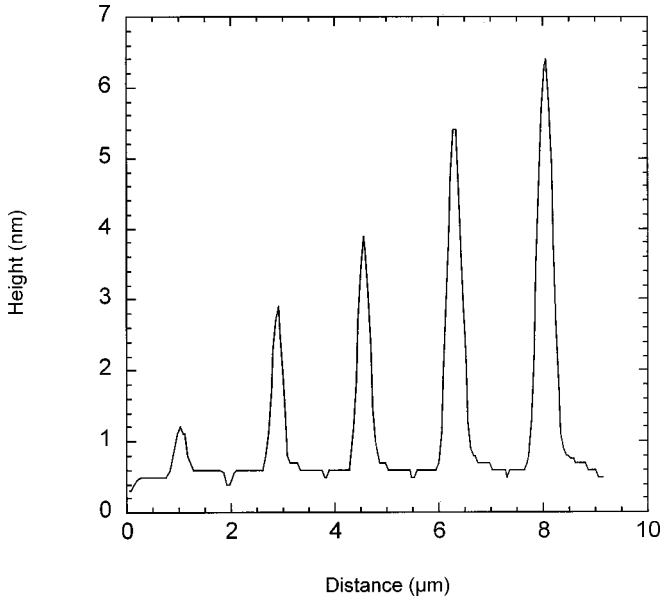

Figure 2. AFM cross section of the E-beam exposure contamination line array of Fig. 1. The increase of height of the lines corresponds to 10, 30, 60, 120, and 180 s E-beam exposure.

After the E-beam treatment, contact to the Si samples was established by smearing InGa eutectic on the back side of the samples. The samples then were pressed against an O-ring of the electrochemical cell leaving a surface containing five 400 × 400 µm openings exposed to the electrolyte. The electrolyte was a 1 M KCN + 0.01 M $KAu(CN)_2$ solution prepared from reagent grade chemicals and deionized water. The electrochemical setup consisted of a conventional three-electrode configuration with a platinum gauze as a counter electrode and a Haber-Luggin capillary with a Ag/AgCl electrode as a reference electrode.

Polarization curves (with a pointwise step rate of 1 mV/s) and potential step experiments were carried out using a Jaissle potentiostat-galvanostat (IMP 88PC-100V).

Chemical characterization of deposits was carried out using Auger electron spectroscopy (AES) using the C peak at 270 eV and the Au peak at 70 eV. AES spectra were acquired on a Perkin Elmer 660 AES spectroscope. For topographic characterization atomic force microscopy (AFM) was employed. AFM profiles were measured in air with an Autoprobe CP from Park Scientific Instruments using silicon ultralever tip in the contact mode at a scanning rate of 1 line per second (lps). SEM images were acquired with the microscope described above.

Results and Discussion

Deposition of C-masks.—Figure 1 shows an AFM top view of a silicon surface that was E-beam line exposed at different equidistantly spaced locations for 10, 30, 60, 120, and 180 s, respectively. Clearly, the five deposited locations can be observed as lines. In order to evaluate the topography of the deposited structures in more detail, an AFM cross section (Fig. 2) was taken through Fig. 1. It is apparent that independent of the exposure time, the lines are distinctly separated. An increase in exposure time results primarily in an increased height and width of the lines. Figure 3 shows the height and the width of the carbon lines in dependence of the E-beam exposure time. The height value was taken at the maximum and the linewidth was defined as full width at half-maximum (FWHM) of the Gaussian cross section. The figure shows that under the present experimental conditions neither height nor width depend linearly on the exposure time. The linewidth of the deposit increases with the irradiation time and then tends to reach a limit value around 330 nm. The fact that the base of the peaks is asymmetric can be ascribed to a nonoptimized astigmatism setting at the SEM. The fact that a higher deposit growth rate is observed for short exposure times can be ascribed to the decomposition of hydrocarbon molecules adsorbed on the substrate: during the first seconds of E-beam exposure the decomposition of a large number of molecules adsorbed on the silicon surface, due to environmental contamination, may instantaneously be converted into a deposit whereas at longer exposure times growth depends only on the pressure of the chamber and thus on the rate of hydrocarbons that are transported through the vacuum and are freshly adsorbed on the irradiated area. During the experiment, the aspect (width/height) ratio changes from 180 for 10 s to 50

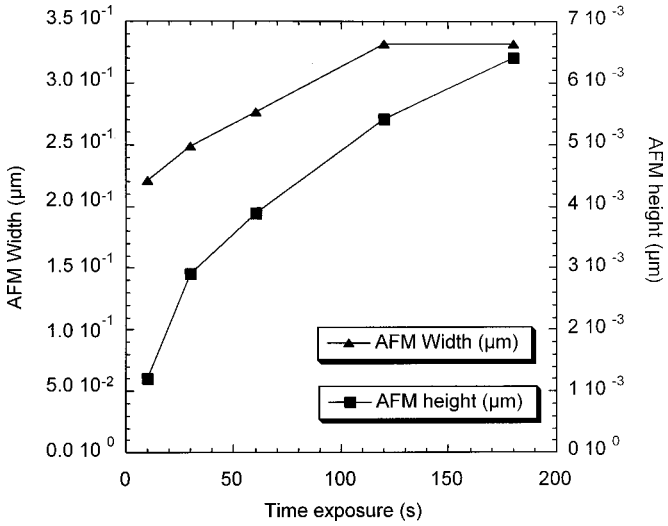

Figure 3. Dependence of the carbon line height and width on the E-beam exposure time.

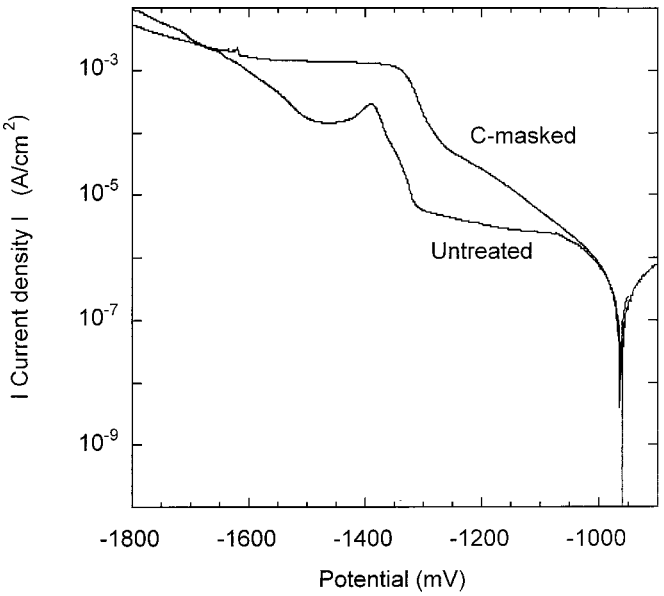

Figure 4. Potentiodynamic polarization curves in the cathodic direction from −0.9 to −1.8 V (Ag/AgCl) (scan rate = 1 mV/s) in 10 mM $KAu(CN)_2$ + 1 M KCN for an untreated Si sample and a sample carrying C-lines patterns as in Fig. 1.

for the longest exposure time. These findings are in line with work aiming for E-beam induced 3-D nanostructure fabrication where at higher contamination contents in the vacuum chamber and longer exposure times needles with width to height ratios ≪1 can be grown.[12]

In order to characterize the carbon distribution over the surface, the intensity of the Auger C peak was acquired as a function of the distance perpendicular to the deposited lines. The Auger results have to be taken in a semiqualitative manner as the Gaussian probing beam is convoluted with the Gaussian shape of the C-lines and additional C-contamination occurs during observation in the AES system. However, the results clearly indicate the presence of the carbon lines.

Electrochemical deposition.—Figure 4 shows cathodic potentiodynamic polarization curves from −0.9 V to −1.8 V (Ag/AgCl) in 10 mM $KAu(CN)_2$ + 1 M KCN for a n-type silicon sample carrying the same carbon line patterns as in Fig. 1. In the figure also, a cathodic polarization curve of an untreated sample is included as a reference. For both samples, the current increases steeply at approximately −1.3 V (Ag/AgCl) to −1.4 V (Ag/AgCl) corresponding to nucleation and growth of gold on silicon. The second current increase at approximately −1.5 V can be attributed to H_2 evolution. It should be noted that in order to achieve metal electrodeposition on the semiconductor surface under cathodic polarization, n-type Si was used. (For p-type material a blocking Schottky junction would be established at the semiconductor/electrolyte interface, which would complicate the electrochemical process).

In order to evaluate whether or not such carbon patterns can be exploited as a mask for electrodeposition, a series of experiments under different electrochemical conditions was carried out. Si samples with arrays of five contamination lines, prepared under the same conditions as in Fig. 1, were electrochemically treated at different potentials and deposition times. Figures 5a-d show the SEM images of the Au deposits obtained after polarization under different conditions.

It is apparent that the surface is covered by a Au deposit except for lines that correspond to the location of the carbon lines. Therefore it is evident that this C-contamination line acts as a mask to the electrodeposition of metal and thus constitutes a negative resist if a sufficient contamination layer is present.

This resist effect can be explained in terms of resistivity of the carbon deposit. It has been reported in literature[17] that the carbon layers produced during E-beam carbon deposition show an amorphous structure, more specifically, DLC is deposited, consisting of a predominant amount of C sp^3. The properties of DLC strongly depend on the C sp^3 content. The high amount of C sp^3 in the deposit leads to electrical properties comparable to diamond. Therefore, in comparison with the resistivity of the n-Si (1-10 Ω cm) DLC behaves as an insulator and as a result suppresses electrodeposition.

From Fig. 5 it is clear that electrodeposition for 30 s at a relatively low potential (−1.3 V, Fig. 5a) results in a rough deposit. The size of the Au clusters is in the range of 100 nm. Further, a poor lateral resolution at the edge of the lines is achieved and the deposit is not entirely covering the silicon surface. The homogeneity of the gold deposit formed between the carbon wires decreases with increased E-beam exposure time; between the carbon lines created by 2 and 3 min E-beam exposure, only few Au crystallites are deposited. This finding hence indicates that electrodeposition may be influenced by the overlap of the Gaussian tails of the contamination lines; with longer E-beam exposure time this overlap increases and hence may for the highest E-beam doses be sufficient to partially suppress the electrodeposition of gold. Using a higher potential of deposition (−1.6 V) results in a smooth continuous gold film onto the silicon surface, as shown in Fig. 5b. The typical feature size of the Au clusters is in the range of 50 nm. The higher potential also leads to a better lateral resolution at the carbon edgelines. Further, at the higher deposition potential the above mentioned insulating effect between the single contamination lines does not occur any more. When potentials cathodic to −1.6 V (Ag/AgCl) are applied, for a longer period of time, overgrowth of the C-lines occurs. Furthermore, and more important, significant hydrogen evolution sets in. As a result, H_2 bubbles sticking to the surface exhibit a masking effect, *i.e.*, lead to a very inhomogeneous deposit.

Figures 5c,d show the SEM images for a shorter (5 s) and a longer (45 s) time of electrodeposition at a deposition potential of −1.6 V (Ag/AgCl) than in Fig. 5b. The shorter deposition time leads to a formation of a continuous film with a remarkable smoothness. The typical feature size is 10 nm. The carbon lines again act as negative resist and the growth of fine and regular crystallites on both sides of the C-lines leads to an excellent lateral resolution. Note that under these conditions, even the finest C-line of a height of only 1 nm (see AFM profile of Fig. 2) is clearly resolved and does not suffer from overgrowth. Deposition for a longer polarization time (Fig. 5d) results in a rough film with typical feature sizes of 100 nm. The lateral resolution is poor due to the overgrowth of crystallites at the C-deposit edges: this effect is of course most affecting the resolution of the smallest contamination line, *i.e.*, the line has almost disappeared after the electrochemical experiment.

In order to investigate the influence of deposition time on the topography in more detail, AFM profiles were measured on the deposits of the samples of Fig. 5 polarized for 5, 30, and 45 s at the applied potential of −1.6 V (Ag/AgCl). The profiles are shown in Fig. 6. The absence of gold deposition can be clearly seen by the ''negative'' peaks. The depth of the widest groove increases roughly from 20 nm to 50 nm from the 5 s sample to the 45 s sample indicating the growth of the Au layer with deposition time. However, due to the high height/width ratio of the deposit, exact imaging of the grooves is not possible as the AFM tip and/or feature convolution occurs. For the 5 and 30 s deposition time the depth reaches with increasing groove width a limiting value of approximately 20 and 50 nm. For 45 s no limiting value is apparent, thus for this sample it is likely that the tip does not reach the substrate even for the widest groove. Nevertheless, the AFM profiles indicate that the longer the deposition time, the rougher the gold film becomes. The root mean square roughness for the deposited films (taken on a C-line free part of the AFM images) increases from 2.1 nm for 5 s to 5.1 nm for 30 s and to 6 nm for 45 s; this is in agreement with the increase in the typical feature sizes observed in the SEM. The deposits obtained for 5 and 30 s polarization time (Fig. 6a and b) show

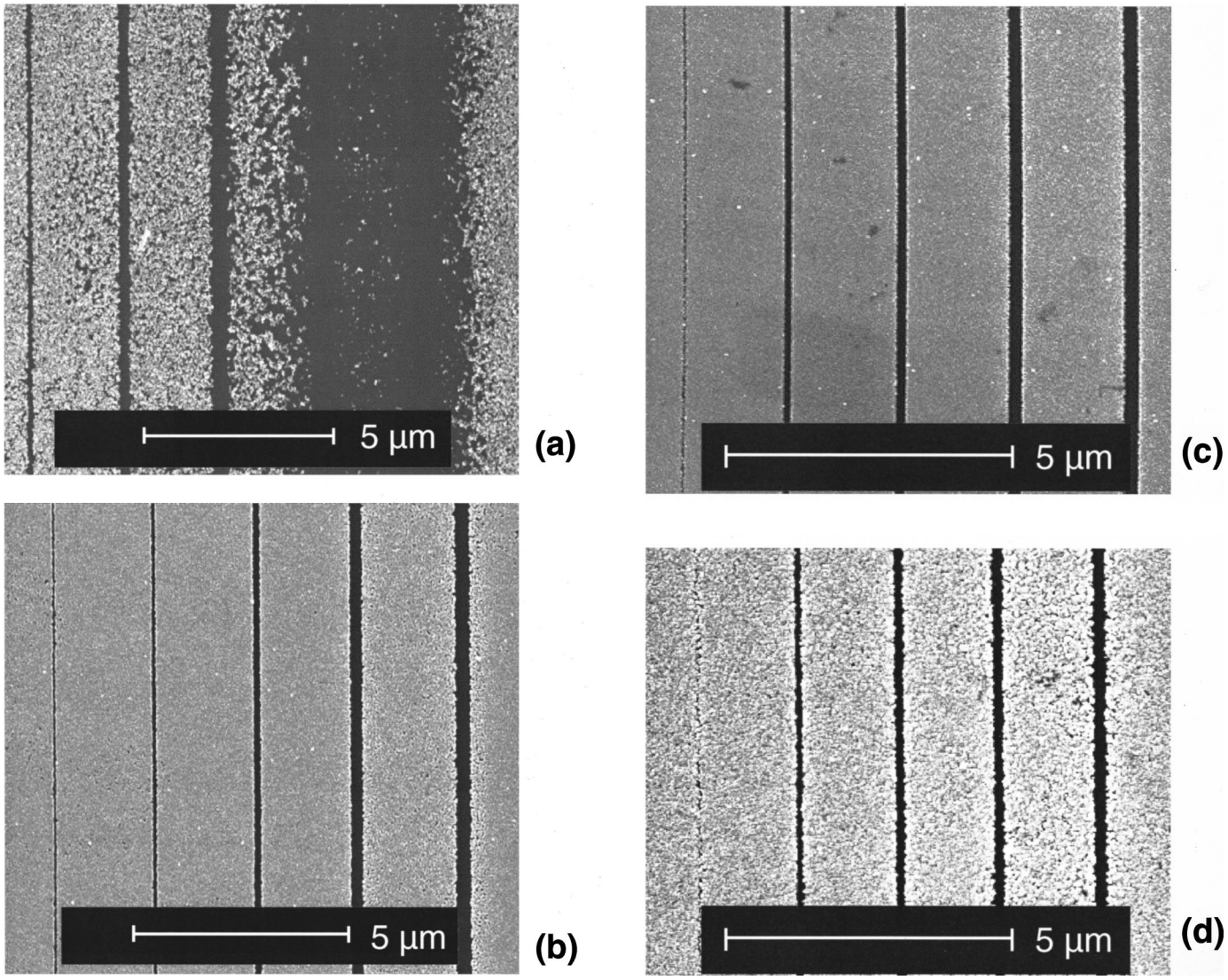

Figure 5. SEM images of Au deposits produced under different electrochemical conditions on Si surfaces carrying the C-lines pattern of Fig. 1. Au deposition was carried out in 10 mM $KAu(CN)_2$ + 1 M KCN by potential steps: (a) to −1.3 V, for 30 s (b) to −1.6 V, for 30 s (c) to −1.6 V, for 5 s (d) to −1.6 V, for 45 s.

that carbon linewidths are not significantly affected by the duration of the electrodeposition except for the smallest C-line which tends to disappear due to coverage or overgrowth by gold. From the AFM profile it is apparent that at the edge of a masking C-line a significantly thicker deposit is formed; This thickening is in agreement with the increased brightness of the edges of the line in the SEM that results from an increased secondary electron emission due to a thicker deposit. This effect becomes more significant for lines obtained by longer E-beam exposure times. Thus it appears as if the C-line edges stimulated the growth of Au. This growth stimulating effect is further in line with the finding of Fig. 4 that in the potential region between −1 V and −1.3 V (Ag/AgCl), the current obtained on the C-line sample is significantly higher than the current measured on the untreated substrate. At present, the cause for this effect is not clear. Speculatively, it may be a geometrical effect based on the current distribution, local diffusion profiles, or be due to adatom mobility, or a plain catalytic effect.

It should be pointed out that in experiments performed with longer deposition time than 1 min at −1.6 V (Ag/AgCl), a series of undesired effects occurred. Not only did, as expected, overgrowth of the C-lines take place, but additionally the Au deposit layers showed some degree of disbonding.

In order to further elucidate the chemical selectivity of this masking technique for electrodeposition, a polarization experiment was carried out on a Si sample, where a rectangle-shaped carbon pattern (around 20 × 30 µm) was produced using the ''full frame mode'' of the SEM. After gold deposition by a polarization curve from −0.9 V to a potential of −1.6 V (Ag/AgCl), an AES line scan for C and Au was acquired through the pattern. The result clearly showed a perfect selectivity, *i.e.*, no Au deposition within the C-rectangle was detectable.

Some aspects of above results should be regarded in the light of the fact that for metal deposition on semiconductor surfaces, the interaction between metal adatoms and intact semiconductor surface is typically weak and hence the deposition follows a 3-D island growth mechanism[24] and implies a growth kinetics of the Volmer-Weber type.[31] Therefore, a sufficiently large cathodic potential is required to create a high density of nuclei leading to an early coalescence of islands. This is in line with the fact that at lower potentials a much rougher deposit and isolated globular features were observed (Fig. 5a), indicating that less nuclei were triggered at the lower potential. At the higher potential, a sufficiently high density of nuclei is triggered to allow coalescence of islands. The fact that at

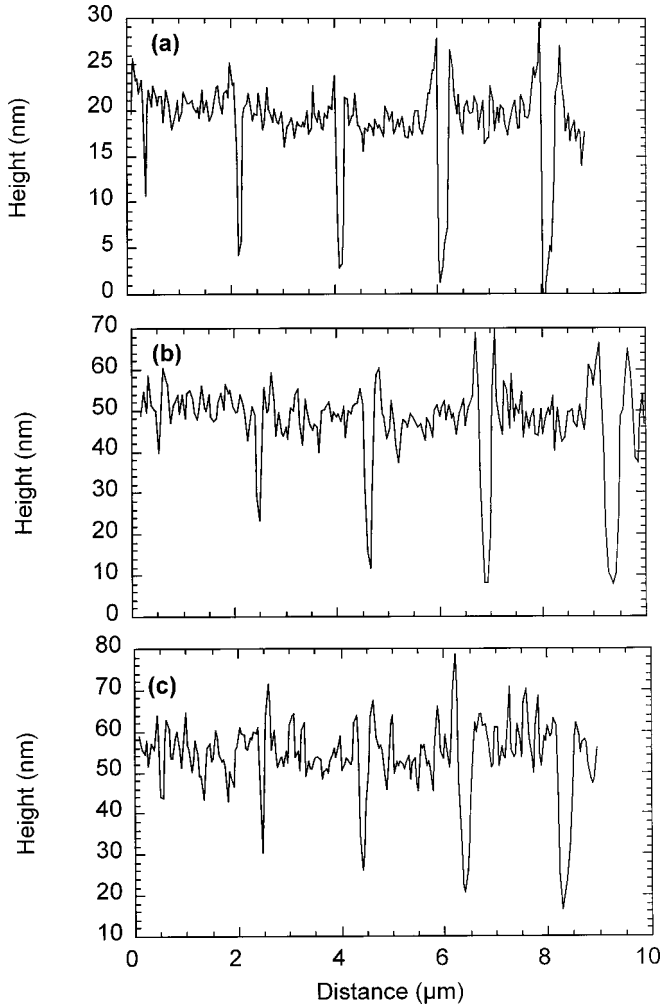

Figure 6. AFM height profiles of deposit obtained in Fig. 5 for (a) 5 s, (b) 30 s, and (c) 45 s at −1.6 V (Ag/AgCl).

−1.6 V a longer polarization time results in a rougher film can be ascribed to a switch from charge transfer to mass transport control as suggested by the corresponding current *vs*. time curves.

To exposure the lower size limit of the deposition process, a series of experiments was performed by minimizing the distance between parallel C-lines, or by producing two perpendicular arrays of six lines which were written with a decreasing spacing. Deposition of gold was performed by applying a potential step to −1.6 V (Ag/AgCl) for 10 s. In all cases the features showed coherent deposition and complete separation by the resist lines. Figure 7 shows an example of the best resolution attained so far where the two parallel C-lines lead to a confined Au deposit line with a width of approximately 90 nm. It has to be pointed out that possibly even smaller structures could be achieved as the result of Fig. 7 corresponds to our minimum experimental E-beam displacement of 200 nm rather than another limiting factor.

Conclusions

The results clearly demonstrate that E-beam induced C-masking of a semiconductor surface can be exploited for a subsequent selective electrochemical metal deposition in the submicrometer range.

E-beam bombardment is used to achieve the decomposition of residual hydrocarbon molecules present in an SEM chamber, to form a carbon-rich deposit. Compared to silicon, the resistivity of this C-deposit is very high and thus it can act as an insulator and locally hinder electrochemical reductions such as in our case the deposition of gold. This novel negative lithographic process depends

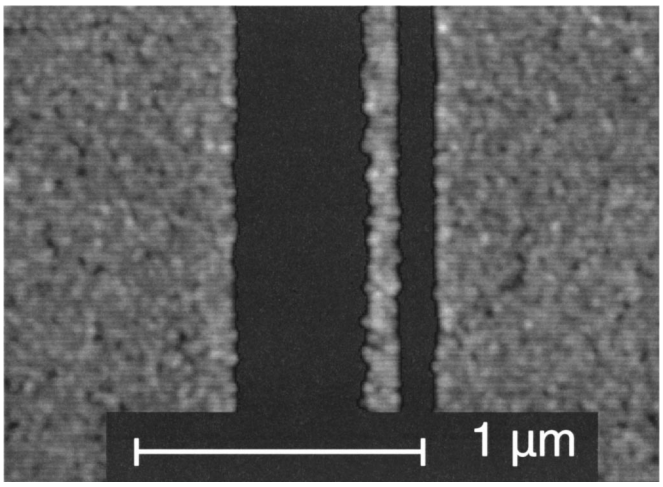

Figure 7. SEM image of a 90 nm wide gold line between two masking C-lines. Au deposition was carried out in 10 mM $KAu(CN)_2$+1 M KCN by a potential step to −1.6 V (Ag/AgCl) for 10 s.

on C-line deposition parameters as well as electrochemical parameters. It has been shown that at C-levels in pressure range of 3×10^{-6} mbar C-masks of a thickness in the 1 nm range can be produced. This layer thickness can be sufficient to efficiently and selectively block the subsequent electrochemical deposition. The electrodeposition of Au on Si shows a 3-D growth morphology suggesting a Volmer-Weber type of island growth mechanism.

To obtain a coherent Au deposition with a high lateral resolution and a high deposition selectivity, deposition potential and time play a crucial role. In general it was found that higher cathodic potential steps for a short period of time lead to more satisfactory results than longer exposure at less cathodic values. This is consistent with the Volmer-Weber approach, suggesting a higher number of activation sites being triggered with a higher overvoltage. This leads to a coalescence of islands in an earlier growth stage, and thus a finer grain size, and, in our case, to a higher achievable lateral resolution.

This process presented in this work opens new perspectives for selective electrodeposition and patterning of surfaces. The process should be applicable to essentially any material that can be electrodeposited from an aqueous environment and thus may be employed to deposit selectively a large palette of materials in the nanometer scale.

Acknowledgment

The authors would like to acknowledge the Swiss National Science Foundation for financial support of this work. For help with the experiments we would like to thank Nicolas Xanthopoulos (EPFL) for AES measurements.

The University of Erlangen-Nuremberg assisted in meeting the publication costs of this article.

References

1. S. M. Sze, *Semiconductor Devices, Physics and Technology*, John Wiley & Sons. Inc., New York (1985).
2. D. V. Averin, and K. K. Likharev, *Mesoscopic Phenomena in Nanostructures*, B. L. Altshuler, P. A. Lee, and R. A. Web, publishers, Amsterdam (1991).
3. *Proc. SPIE-Int. Soc. Opt. Eng.*, **1465** (1991); *Proc. SPIE-Int. Soc. Opt. Eng.*, **1671** (1992); *Proc. SPIE-Int. Soc. Opt. Eng.*, **1924** (1993); *Proc. SPIE-Int. Soc. Opt. Eng.*, **2194** (1994); *Proc. SPIE-Int. Soc. Opt. Eng.*, **2437** (1995); *Proc. SPIE-Int. Soc. Opt. Eng.*, **2723** (1996).
4. D. R. Allee, and A. N. Broers, *Appl. Phys. Lett.*, **57**, 2271 (1990).
5. X. Pan, D. R. Allee, A. N. Broers, Y. S. Tang, and W. Wilkinson, *Appl. Phys. Lett.*, **59**, 3157 (1991).
6. T. O. Sedgwick, A. N. Broers, and B. J. Agule, *J. Electrochem. Soc.*, **119**, 1769 (1972).
7. D. R. Allee, C. P. Umbach, and A. N. Broers, *J. Vac. Sci. Technol. B*, **9**, 2838 (1991).

8. H. G. Craighead, R. E. Howard, L. D. Jackel, and P. M. Mankiewich, *Appl. Phys. Lett.*, **42**, 38 (1982).
9. U. Dötsch, and A. D. Wieck, *Nucl. Instrum. Methods Phys. Res. B*, **139**, 12 (1998).
10. T. K. Whidden, J. Allgair, J. M. Ryan, M. N. Kozicki, and D. K. Ferry, *J. Electrochem. Soc.*, **142**, 1199 (1995).
11. H. W. P. Koops, J. Kretz, M. Rudolph, M. Weber, G. Dahm, and K. L. Lee, *Jpn. J. Appl. Phys.*, **33**, 1, 7099 (1994).
12. M. Komuro, and Hiroshima, *Microelectron. Eng.*, **35**, 273 (1997).
13. N. Miura, H. Ishii, J. Shirakashi, A. Yamada, and M. Konagai, *Appl. Surf. Sci.*, **113/114**, 269 (1997).
14. R. F. Voss, R. B. Laibowitz, and A. N. Broers, *Appl. Phys. Lett.*, **37**, 656 (1980).
15. A. N. Broers, W. W. Molzen, J. J. Cuomo, and D. Wittels, *Appl. Phys. Lett.*, **29**, 596 (1976).
16. N. Miura, T. Numaguchi, A. Yamada, M. Konagai, and J. Shirakashi, *Jpn. J. Appl. Phys.*, **36**, L1619 (1997).
17. N. Miura, A. Yamada, and M. Konagai, *Jpn. J. Appl. Phys.*, **36**, L1275 (1997).
18. G. Oskam, D. van Heerden, and P. C. Searson, *Appl. Phys. Lett.*, **73**, 3241 (1998).
19. G. Oskam, J. G. Long, M. Nikolova, and P. C. Searson, *Mater. Res. Soc. Symp. Proc.*, **451**, 257 (1997).
20. P. Bindra, H. Gerischer, and D. M. Kolb, *J. Electrochem. Soc.*, **124**, 1012 (1977).
21. P. Allongue, and E. Souteyrand, *J. Electroanal. Chem.*, **362**, 79 (1993).
22. B. Rashkova, B. Guel, R. T. Pötzschke, G. Staikov, and W. J. Lorenz, *Electrochim. Acta*, **43**, 3021 (1998).
23. G. Oskam, J. G. Long, and P. C. Searson, *J. Phys. D*, **31**, 1227 (1998).
24. E. Budewski, G. Staikov, and W. Lorenz, *Electrochemical Phase Formation and Growth*, VCH, Weinhein (1996).
25. D. Edelstein, J. Heidenreich, R. Goldblatt, W. Cote, C. Uzoh, N. Lustig, P. Roper, T. McDevitt, W. Motsiff, A. Simon, J. Dukovic, R. Wachnick, H. Rathore, R. Schulz, L. Su, S. Luce, and J. Slattery, *Tech. Dig. Int. Electron Devices Meet.*, **773**, 944 (1997).
26. P. C. Andricanos, C. Uzoh, J. O. Dukovic, J. Horkans, and H. Deligianni, *IBM J. Res. Dev.*, **42**, 567 (1998).
27. P. C. Andricanos, *Electrochem. Soc. Interface*, **8**(1), 32 (1999).
28. P. Schmuki, L. E. Erickson, and D. J. Lockwood, *Phys. Rev. Lett.*, **80**, 4060 (1998).
29. K. Uosaki and H. Kita, *J. Electroanal. Chem.*, **239**, 301 (1989).
30. U. Schmidt, S. Vinzelberg, and G. Staikov, *Surf. Sci.*, **348**, 261 (1996).
31. M. Volmer and A. Weber, *Z. Phys. Chem.*, **119**, 227 (1926).